

A Machine Learning-based Calibration of a 1D ejector model from CFD

**Jan Van den Berghe^{a,b}, Jagadish Babu Vemula^b,
Yann Bartosiewicz^b and Miguel Alfonso Mendez^a**

^a von Karman Institute for Fluid Dynamics (VKI),
Waterloosesteenweg 72, 1640 Sint-Genesius-Rode, Belgium, jan.vandenbergh@vki.ac.be, CA.
^b Institute of Mechanics, Materials, and Civil Engineering (iMMC)
Université catholique de Louvain (UCLouvain), 1348 Louvain-la-Neuve, Belgium

Abstract:

Ejectors are devices that expand a primary flow through a nozzle to entrain and compress a secondary flow without moving parts. They can be modelled in 1D as two streams exchanging momentum. However, the engineering modelling of this exchange is based on closure parameters such as friction coefficients that must be calibrated against experimental or numerical data. This work proposes a general machine learning framework for calibrating engineering models governed by Ordinary Differential Equations (ODEs) and presents its application to the 1D modelling of an ejector. We combine a physics-separated approach with a physics-integrated approach, with the first acting as an initial guess for the second. The first approach calibrates shear and friction coefficients from their counterpart extracted via post-processing of an axisymmetric CFD simulation. The second consists of calibrating these coefficients from the prediction of physical quantities (pressures, temperatures, and cross-sections), thus making the training process aware of the ODEs driving the forecast.

Keywords:

1D ejector modelling, closure modelling, physics-constrained machine learning

1. Introduction

Ejectors are flow devices that expand a primary flow to entrain and compress a secondary flow into a mixing pipe. These ‘compressors’ have no moving parts and are thus robust and without limitations on the working fluid (gas, liquid, two-phase). Their applications include aeronautics, the chemical and processing industry, power generation and refrigeration [1].

Ejectors are commonly modelled with 0D lumped parameter formulations [2–6], meaning that conservation laws are expressed between key sections such as the throat and the exit of the primary nozzle, the constant area section of the mixing pipe and the exit of the diffuser. These models give fast predictions of the global performance in the form of mass flow rates but require calibration of several closure coefficients accounting for the isentropic efficiencies of key components. On the other hand, classic CFD provides detailed flow fields [7,8], but requires more computational time and effort for meshing and setting up the solver, which is generally too expensive at system scale. A compromise consists of 1D models, which discretize the flow field in the axial direction. The mixing pipe can be modelled with a single domain [9], or with two interacting domains [10–12]. These models still require calibration, for example, for modelling wall friction and shear. Nevertheless, they provide local information and resolve more physics related to entrainment than 0D models, at a fraction of the cost of 2D/3D CFD.

Closure relations mapping these closure coefficients to physical quantities (e.g., a friction coefficient which depends on the Reynolds number) could make these models self-standing and thus more useful in early design stages, but their derivation is particularly challenging. This work proposes a machine learning formalism to discover such closure relations from data. By training the model on reliable CFD data, the intricacies of the 2D flow field can be lumped into the closure coefficients of the lower dimensional 1D model to maximize the accuracy of these models. This data-driven approach has been successfully applied in other branches of fluid mechanics such as heat transfer or and turbulence modelling. These can be classified as physics-separated (as in [14]) or physics-integrated (as in [15, 16]) depending on whether the learning process is carried out on data extracted from a simulation or during a simulation. These approaches are briefly reviewed in the next section. None of these have been implemented for the calibration of ejector models.

In this work, we propose a general formulation for machine learning-based closure of a system of ordinary differential equations (ODEs), and we apply it to a 1D ejector model with two streams (1D-2s hereafter). The

general framework is presented in section 2. and its application on the ejector model in section 3.. The results are discussed in section 4., leading to the conclusions in section 5..

2. A general framework for machine learning-based calibration

We consider a physical problem governed by a system of ordinary differential equations (ODEs) in the state variables $\mathbf{u} \in \mathbb{R}^{n_u}$ and a set of parameters $\mathbf{p} \in \mathbb{R}^{n_p}$ to be linked to the state variables. In this work, we focus on boundary value problems in $x \in [0, L]$, and denote the sought-after closure relation as $\mathbf{p} = g(\mathbf{u}, x)$. Thus the closure problem can be written as

$$f\left(\mathbf{u}, \frac{d\mathbf{u}}{dx}, \frac{d^2\mathbf{u}}{dx^2}, \dots, x, \mathbf{p} = g(\mathbf{u}, x)\right) = 0, \quad (1)$$

with boundary conditions $\mathbf{u}(0) = \mathbf{u}_L$ and $\mathbf{u}(L) = \mathbf{u}_R$. This framework is general enough to encompass many physical systems, from turbulence modelling [15–18] to general inverse modelling [13]. This work presents the first implementation of this framework for the closure of 1D ejector models.

The problem of finding the unknown function is generally a difficult variational problem. Machine learning offers an alternative approach by approximating the unknown function using a parametric model $\mathbf{p} = g(\mathbf{u}, x; \mathbf{w})$ which depends on a finite set of weights $\mathbf{w} \in \mathbb{R}^{n_w}$. This could range from a simple linear relation to artificial neural networks (ANNs), and the range of possible functions that the given model can represent defines the 'hypothesis set' in the machine learning formalism [21]. Following [19], the identification of the weights \mathbf{w} can be carried out using physics-separated and physics-integrated approaches (see also [14], and [13, 15–18]).

The physics-separated approach is a classic supervised learning formulation which assumes that a set of instances $(\tilde{\mathbf{u}}_i, x_i)$ and the associated parameters $\tilde{\mathbf{p}}_i$ are available. Therefore, the optimal set of weights is the one that minimizes a cost function $J(\mathbf{w})$ such as, for example:

$$J_1(\mathbf{w}) = \sum_i \sum_r \frac{(\tilde{\mathbf{p}}_{i,r} - g(\mathbf{u}_{i,r}, x_i; \mathbf{w}))^2}{\tilde{\mathbf{p}}_{i,r}^2}, \quad (2)$$

where i is the index spanning the instances $\tilde{\mathbf{p}}_i$ at coordinates x_i and r is the index spanning the entries in each vector of parameters (i.e. the closure coefficients that make up \mathbf{p}).

This regression problem is shown schematically in block II of figure 1 and starts with an initial guess \mathbf{w}_0 . The gradient of the cost function $d_w J$ only requires the gradient of the parametric function $d_w g$; this is easily available for usual machine learning models (e.g. using backpropagation in ANNs) hence classic gradient-base optimizer such as the BFGS algorithm [20] can be implemented efficiently. However, this approach requires that both the parameters $\tilde{\mathbf{p}}_i$ and the full states $\tilde{\mathbf{u}}_i$ can be extracted from a sufficiently rich dataset with sufficient accuracy (cf. block I in figure 1). This is rarely possible from experimental data. Moreover, the trained model g is unaware of the underlying physical problem in (1) since the model is never called during training.

The physics-integrated approach includes the physical problem in (1) during the learning process (cf. block III in figure 1). Note that both approaches are self-standing, but can be applied successively. The extraction of the model parameters from data is not required, and the training is based on some observation of the states and the prediction that the model f can achieve for a given set of weights \mathbf{w} . Considering the simplest case of full observation of the states $\tilde{\mathbf{u}}_i$ and denoting the solution of (1) as $\mathbf{u}_i(g(\mathbf{u}_i, x_i; \mathbf{w}))$ when the closure is achieved with the weights \mathbf{w} , the optimal set of weights minimizes a cost function of the form

$$J_2(\mathbf{w}) = \sum_i \sum_r \frac{(\tilde{\mathbf{u}}_{i,r} - \mathbf{u}_{i,r}(g(\mathbf{u}_{i,r}, x_i; \mathbf{w})))^2}{\tilde{\mathbf{u}}_{i,r}^2} \quad (3)$$

where i is the index spanning the instances $\tilde{\mathbf{u}}_i$ at coordinates x_i and r is the index spanning the entries in each state vector (i.e. the variables considered for the cost function definition).

The relative error is preferred here due to the composite nature of common state vectors (e.g., pressures and temperatures). Using the chain rule, it is easy to see that in this formulation, the gradient of the cost function $d_w J$ requires the gradient of the problem solution with respect to the parameters and the gradient of the parameters with respect to the weights, i.e. $d_w J(\mathbf{u}(g(\mathbf{w}))) = d_u J d_p \mathbf{u} d_w g$. Computing this gradient symbolically is challenging and requires adjoint differentiation (cf. [13, 15–18]), but for a computationally inexpensive solver of f and a small number of parameters, a simple finite difference implementation is feasible. Besides avoiding the need for extracting the parameters $\tilde{\mathbf{p}}$ from data, this approach has the main merit of pairing the closure

with the solver with which it is later deployed. On the other hand, the model sensitivity to the parameters ($d_p \mathbf{u}$) strongly influences the cost function gradient and often results in more poorly behaved and multimodal cost functions.

In this work, we propose a combination of the two approaches, whereby the solution of a physics-separated approach is used as a starting point for a physics-integrated approach (hence successively following blocks I to III in figure 1). This offers an excellent balance between accuracy, robustness and computational cost.

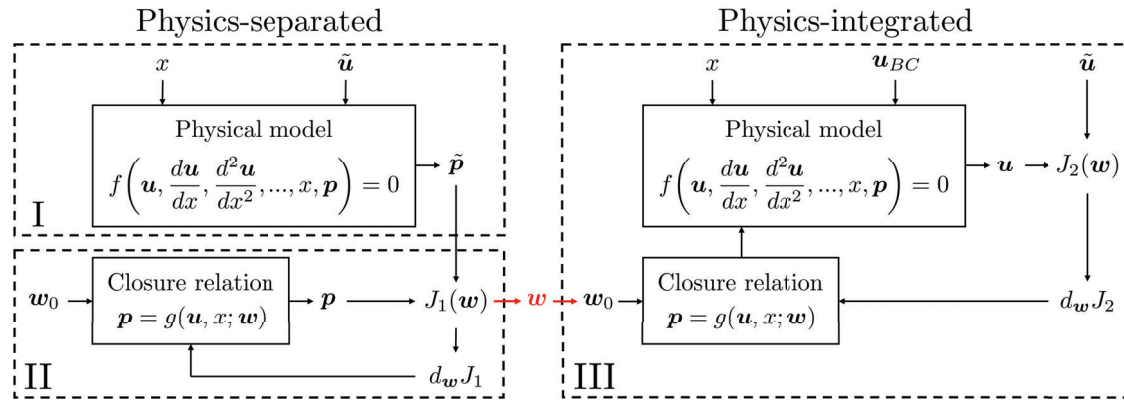


Figure 1: Schematic overview of the physics-separated and the physics-integrated approach for calibrating a physical model f through a closure relation g , given data $\tilde{\mathbf{u}}$. The physics-separated approach consists of (I) extracting the reference parameters $\tilde{\mathbf{p}}$ from data and (II) applying a classic supervised machine learning technique for regressing \mathbf{p} . The physics-integrated approach (III) includes the physical model in the training process and thus requires the sensitivity of the model with respect to its parameters $d_p \mathbf{u}$. Both methods are self-standing, but this work proposes to apply them successively (I-III) as indicated in red.

3. Application to a 1D ejector model

The previously introduced model calibration framework is applied to the modelling of a supersonic ejector using a 1D and two streams formulation. The calibration is based on data from a 2D axisymmetric CFD simulation presented in [22]. This is briefly reviewed in section 3.1.. The model formulation is presented in section 3.2. while the procedure for the calibration is reported in section 3.3..

3.1. The CFD Dataset

We consider an ejector with a converging primary nozzle, operating with total pressures $p_{tp} = 5$ bar, $p_{ts} = 1$ bar and static back pressure $p_b = 2.2$ bar. Herein, the subscripts p and s are used for variables related to the primary and the secondary flows, respectively (see list of symbols at the end of the article). The total temperatures equal $T_{tp} = T_{ts} = 293\text{K}$. The numerical domain and a contour of the Mach number field are shown in figure 2. The primary jet is under-expanded due to the large pressure difference between the inlets, which leads to a shock train in the mixing pipe. This is evidenced by the dividing streamline as indicated by the full red line in figure 2. The ejector operates in off-design conditions, so the maximal flow rate is not reached, and the mixed flow remains subsonic. Consequently, no shock train is present in the diffuser as would be the case in on-design conditions [7]. Interested readers are referred to [22] for further numerical details and the validation against experiments.

The data assimilation in this work focuses on the mixing pipe since the primary and secondary inlets can be accurately described with classic quasi-1D flow theory. The mixing pipe features complex flow phenomena, mixing the two streams and shock trains interacting with shear layers. This portion of the ejector is the one where closure relations are required the most.

The first step in the data preparation consists of calculating the dividing streamline in the mixing pipe. This is defined as the line bounding the primary mass flow rate. Hinging on the axisymmetry of the problem, this is the radius r_{div} such that:

$$\dot{m}_p(x) = \int_0^{r_{div}} \rho(x, r) u(x, r) 2\pi r dr, \quad \text{and} \quad \dot{m}_s(x) = \int_{r_{div}}^R \rho(x, r) u(x, r) 2\pi r dr, \quad (4)$$

The dividing streamline is also used to average the relevant flow variable across the ejector's section, i.e.

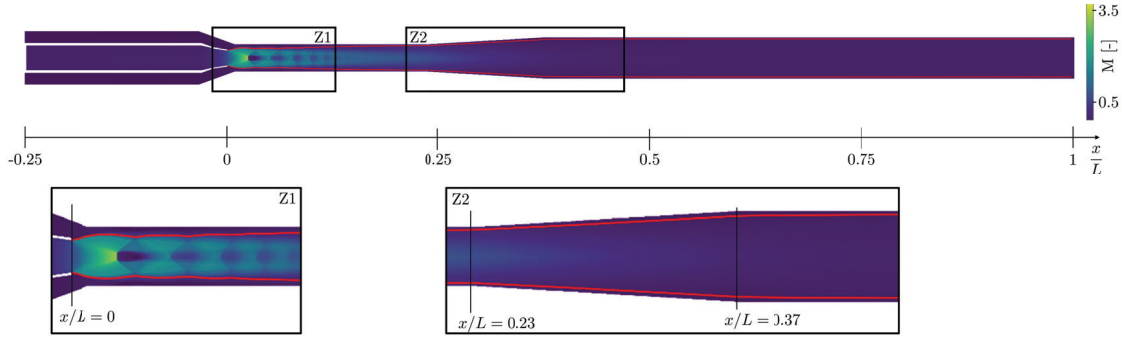


Figure 2: Mirrored Mach number field of an ejector operating in off-design conditions, obtained through classic axisymmetric CFD [22]. A shock train is present in the mixing pipe due to the different static pressures of both streams at the exit of the primary nozzle. The red line indicates the dividing streamline. The reference 1D data in the rest of the work is obtained through averaging over the resulting cross-sections with equations (5).

$$\hat{\rho}_{p,s}(x) = \frac{1}{A_{p,s}} \int_{A_{p,s}} \rho \, dA_{p,s}, \quad \hat{u}_{p,s}(x) = \frac{1}{\hat{\rho}_{p,s} A_{p,s}} \int_{A_{p,s}} \rho u \, dA_{p,s}, \quad \text{and} \quad \hat{e}_{t,p,s}(x) = \frac{1}{\hat{\rho}_{p,s} A_{p,s}} \int_{A_{p,s}} \rho e_t \, dA_{p,s}, \quad (5)$$

where the hat $\hat{\cdot}$ denotes the cross-section averaged variables and the subscripts p, s denote the primary and the secondary stream. Therefore, the areas $A_{p,s}$ are the portion of the domain corresponding to $r \in [0, r_{div}]$ and $r \in [r_{div}, R]$ respectively. It is worth noticing that the specific choice of density average is arbitrary, but the other two equations enforce that the 1D variables keep the same mass flow rate and total internal energy as the CFD [23]. The final dataset consists of the cross-sections $A_{p,s}$ and the flow variables obtained with equation 5 at 1530 spatial coordinates x of the single CFD simulation shown in figure 2. Hence, the available data is locally rich, but limited to a single geometry and a single operating condition. Therefore, the resulting calibration in section 4. can not be expected to generalize to different operating conditions.

3.2. Model definition

The main idea of the 1D- two stream ejector model is to treat the inlets as 1D domains with the variable area along the axial coordinate x (as in the 1D modelling of nozzle flows). The mixing pipe is modelled as a 1D domain with 2 streams that exchange momentum through shear and with the wall. The division of the complete section between the two streams remains a degree of freedom, e.g., the same primary mass flow rate can pass through a narrow or a wide flow passage, with the secondary cross-section adapting accordingly. Therefore, the static pressure is assumed to be equal in both streams as an additional constraint. This set of equations is known as the compound flow theory, originally proposed by Bernstein [24] and adopted later in ejector modelling [6, 10, 23, 25]. The set of ODEs (1) consists of the following governing equations:

$$\frac{d_x \rho}{\rho} = \frac{1}{\beta} \left(d_x A + \frac{1}{2} f_{ps} l_{ps} \frac{(M_p^2 - M_s^2)^2}{M_p^2 M_s^2} - \frac{1}{2} f_w l_w (1 + (\gamma - 1) M_s^2) \right), \quad (6)$$

$$\frac{d_x \rho_{tp}}{\rho_{tp}} = -\frac{1}{2} \frac{f_{ps} l_{ps}}{A_p} \gamma (M_p^2 - M_s^2), \quad (7)$$

$$\frac{d_x \rho_{ts}}{\rho_{ts}} = \frac{1}{2} \frac{f_{ps} l_{ps}}{A_s} \gamma (M_p^2 - M_s^2) - \frac{1}{2} \frac{f_w l_w}{A_s} \gamma M_s^2, \quad (8)$$

$$\frac{d_x T_{tp}}{T_{tp}} = 0 \quad \text{and} \quad \frac{d_x T_{ts}}{T_{ts}} = 0, \quad (9)$$

$$\frac{d_x A_p}{A_p} = \left(\frac{1 - M_p^2}{\gamma M_p^2} \right) \frac{d_x \rho}{\rho} + \frac{1}{2} \frac{f_{ps} l_{ps}}{A_p} \left(1 + (\gamma - 1) M_p^2 \right) \left(1 - \frac{M_s^2}{M_p^2} \right), \quad (10)$$

$$\frac{d_x A_s}{A_s} = \left(\frac{1 - M_s^2}{\gamma M_s^2} \right) \frac{d_x \rho}{\rho} - \frac{1}{2} \frac{f_{ps} l_{ps}}{A_s} \left(1 + (\gamma - 1) M_s^2 \right) \left(\frac{M_p^2}{M_s^2} - 1 \right) + \frac{1}{2} \frac{f_w l_w}{A_s} (1 + (\gamma - 1) M_s^2), \quad (11)$$

where

$$\beta = A_p \frac{1 - M_p^2}{\gamma M_p^2} + A_s \frac{1 - M_s^2}{\gamma M_s^2}, \quad (12)$$

and with the constraint that $A_p + A_s = A$. It is worth noticing that eq. (6) implies that the static pressure is equal on both primary and secondary sides, i.e. $p_p = p_s = p$. The derivation of these equations from conservation principles is presented in appendix A. We refer to the list of symbols for the definition of all variables.

The two closure parameters to be identified in a data-driven model calibration are the shear coefficient f_{ps} between the streams and the wall friction coefficient f_w . These are linked to the shear forces acting on the perimeter of the primary cross-section (l_{ps}) and the wall's perimeter (l_w), respectively. Therefore, in the formalism introduced in section 2., these variables constitute the model parameters $\mathbf{p} = [f_{ps}, f_w]^T$ to be provided by the closure function g while the state variables are $\mathbf{u} = [\rho, \rho_{lp}, \rho_{ts}, T_{lp}, T_{ts}, A_p, A_s]^T$. The local Mach numbers can be computed from these variables (e.g. the static and total pressures) or the local densities using the ideal gas law. Note that the constraint on the cross-sections can be imposed by first calculating the gradient of the primary cross-section A_p and subtracting it from the gradient of the total cross-section.

It is worth stressing that the assumption of equal static pressure is problematic at the inlet of the mixing pipe because the primary flow is generally under-expanded (cf. figure 2). Therefore, the proposed model cannot be used from the exit of the primary nozzle ($x = 0$) unless a pressure equalization mechanism is introduced in the model. Alternatively, the areas for the primary and secondary flows must be provided at the inlet of the mixing channel: in this case, the pressures naturally equalize within a short distance from the inlet; this is akin to what happens through the shock cells in the CFD simulation. The development of the first approach is left to future work. In this work, we use the dividing streamline identified from the CFD up to the point where the pressures equalize, and downstream, we use the compound equations (6)-(12) (this is further discussed in Section 4.)

The research question addressed in this work is the feasibility of deriving the spatial distribution of shear and friction coefficients that makes the 1D model comply with the post-processed CFD data. Moreover, in this work, we do not (yet) link the closure parameters to the state, which is a more complex task and should be studied across a wide range of operating conditions. We focus on the parameters' spatial distributions and their derivation by implementing the physics-separated and physics-integrated approaches.

3.3. Calibration

Physics-separated approach

Following the framework in Section 2., the physics-separated approach consists of calculating the closure coefficients from the processed CFD data. To this end, equations (7) and (8) can be used to compute the 1D shear and friction coefficients (f_{ps} and f_w) if all the other terms are extracted from data via appropriate processing. These two equations give:

$$f_{ps} = -\frac{2A_p}{l_{ps}\gamma(M_p^2 - M_s^2)} \frac{d_x p_{lp}}{p_{lp}} \quad \text{and} \quad f_w = -\frac{2A_s}{l_w\gamma M_s^2} \left(\frac{d_x p_{ts}}{p_{ts}} - \frac{1}{2} \frac{f_{ps} l_{ps}}{A_s} \gamma (M_p^2 - M_s^2) \right). \quad (13)$$

Both definitions rely on the differentiation of pressure evolution, computed using finite differences on a smoothed version of the signal. The derivation was carried out with a second-order centred scheme, while the smoothing was carried out with a Savitzky-Golay filter with a second-order polynomial. The resulting closure coefficients are, therefore, functions of the spatial coordinate x and could be linked to the local value of the state variables \mathbf{u} , or local values of dimensionless numbers such as Reynolds and Mach numbers in each stream, or pressure and temperature ratios. However, this regression has a high risk of overfitting because the flow field (and thus the closure coefficients) can change drastically with the operating conditions. This challenging regression requires a large dataset and is foreseen for future work. This work focuses on a single off-design operating point, with regression as a function of the axial coordinate x . Practically, we minimize the cost function (2) separately for the shear and the wall friction coefficient with a parametric function g heuristically constructed after analyzing the data. The specific choice is provided in Section 4.1.. Note that we can split the regression in two smaller problems because the predicted closure coefficients \mathbf{p} can be evaluated independently against their references $\tilde{\mathbf{p}}$.

Physics-integrated approach

The closure coefficients derived in the previous section are those that minimize the error in the definitions (13), but this does not guarantee that the model prediction is the most accurate. The complex interplay of this parameter with the other equations in the model (6)-(11) introduces additional sensitivities to the model prediction. The physics-integrated approach seeks to account for all of these using the cost function (3) to penalize model prediction (that indirectly depends *also* on the parameters). In the investigated calibration problem, the observed quantities included in the cost function are the pressures p_{lp} and p_{ts} and the cross-sections A_p and A_s . The static pressure p is not included because the shock trains make p_p and p_s oscillate. Since the 1D model can only reproduce the mean trends due to the assumption of equal static pressures, this oscillation could unfairly penalize the model prediction and produce local minima in the cost function landscape. Moreover, the total temperature is excluded because it is assumed to be constant in the mixing pipe and

thus does not contribute to accentuating the cost function gradient distribution along the spatial coordinate. Finally, an additional term is added at the exit ($x = L$) to penalize the potential error on the back pressure. This penalization helps enforce the boundary condition of the model. Therefore, the cost function (3) for this approach becomes

$$J_2(\mathbf{w}) = \sum_i \left[\frac{(\bar{p}_{p,i} - p_{p,i}(g))^2}{(\bar{p}_{p,i})^2} + \frac{(\bar{p}_{s,i} - p_{s,i}(g))^2}{(\bar{p}_{s,i})^2} + \frac{(\bar{A}_{p,i} - A_{p,i}(g))^2}{(\bar{A}_{p,i})^2} + \frac{(\bar{A}_{s,i} - A_{s,i}(g))^2}{(\bar{A}_{s,i})^2} \right] + \frac{\bar{p}(L) - p(g, L)}{\bar{p}(L)} \quad (14)$$

where the summation is carried out over the available instances (e.g. grid points in x), the functional dependency on g denotes the model prediction based on the closure g and the summation over the index r is made explicit over the four variables involved. We recall that the closure function depends on weights \mathbf{w} , i.e. $g := g(x, \mathbf{w})$. For a given guess of the weights, hence a given closure law $\mathbf{p} = g(x, \mathbf{w})$, the cost function $J_2(\mathbf{w})$ in (14) is computed by first solving numerically the set of equations in (6)-(11) using a shooting method.

4. Results

4.1. Physics-separated approach

Figure 3 shows the original and filtered 1D distributions of the total pressure in both streams from the post-processed CFD, from the exit of the primary nozzle at $x/L = 0$ to the exit of the numerical domain at $x/L = 1$ (cf. equations (5)). The total pressures equalize for $x/L > 0.4$, as a result of the mixing process and the growth of the shear layer separating the two streams. After this equalization, the two streams are fully mixed and indistinguishable, driven by a common total pressure and temperature. The zoom Z1 (shown on the right) displays a sharp drop in total pressure at $x/L = 0.025$. This corresponds to the Mach disk in figure 2. This is a 2D effect which can not be reproduced by the 1D model and is thus better filtered out before the data is used for calibration. The filtered signal thus ‘averages’ the shock train for the computation of the closure coefficients. The window length of the Savitzky-Golay filter has been tuned to this end.

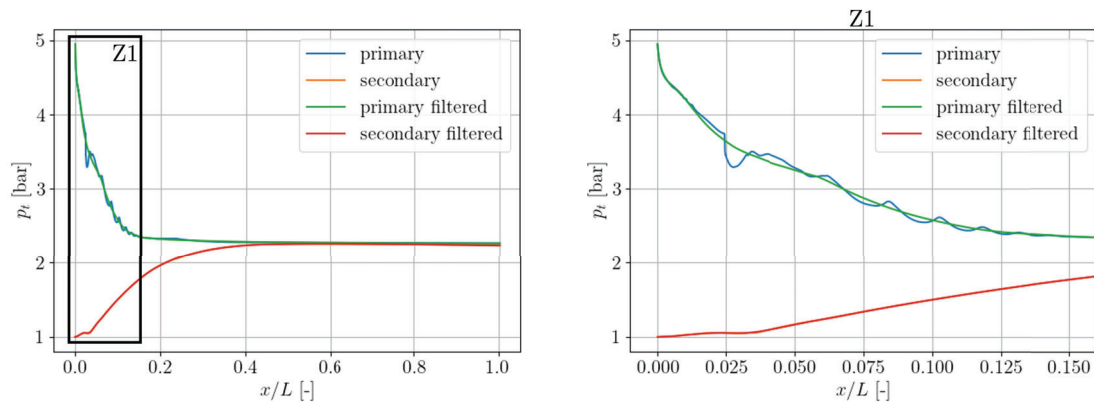


Figure 3: Filtering of the 1D total pressure field obtained through post-processing the CFD simulation in figure 2. The total pressures tend towards a common value as the primary and secondary streams exchange momentum. The shock train at the inlet of the mixing pipe strongly affects the primary total pressure, which is therefore filtered with a Savitzky-Golay filter before being differentiated (cf. equations (13)). The filtered secondary total pressure coincides with its raw counterpart since it is already quite smooth.

The shear and friction coefficients computed with equations (13) are shown in figures 4 and 5 respectively. The unfiltered coefficients show a sharp peak at the position of the Mach disk, as the primary total pressure changes suddenly at this point. This artefact is avoided through filtering. Still, both results indicate large coefficients at the inlet of the mixing pipe, especially in the wall friction f_w , which reaches an extreme value of 25 (with values expected to be of the order 0.01). A possible explanation could be the separation region behind the wall between the exit of the primary nozzle and the secondary inlet. This trailing edge is not sharp, so it is followed by a region of separated flow which slows down both the primary and the secondary stream through shear. This effect is locally quite strong for the primary flow due to a momentum deficit between the sonic flow and the stagnant flow in the bubble, hence a large value of the shear coefficient f_{ps} . However, this force is applied equally but with an opposite sign on the secondary flow, which therefore tends to *accelerate* rather than *decelerate*. In turn, a high wall friction coefficient is thus needed to overcome this numerical acceleration and still represent the actual friction forces on the secondary stream.

The peak at the inlet of the mixing domain shows an exponential decay, so an exponential function is chosen in the parametric closure function g for the calibration. Downstream, the evolution is rather flat, except for the oscillations induced by the shock train. Therefore, the closure function g is parametrized with a linear trend downstream. This leads to the following parametric function with 5 weights:

$$\begin{cases} y = w_1 + w_2 \exp(-w_3 x) & \text{if } x \leq w_0 \\ y = w_1 + w_2 \exp(-w_3 w_0) + w_4 x & \text{if } x > w_0 \end{cases} \quad (15)$$

This function is used for both closure coefficients, bringing the number of weights to 10. The mismatch with the post-processed coefficients is minimized using the summed squared error as a cost function and with the BFGS algorithm available in SciPy [20]. The gradient computation is performed with finite differences, which is affordable due to the low cost of the function to be called and the low number of weights. The resulting regression is shown alongside the raw and the filtered signals in figures 4 and 5.

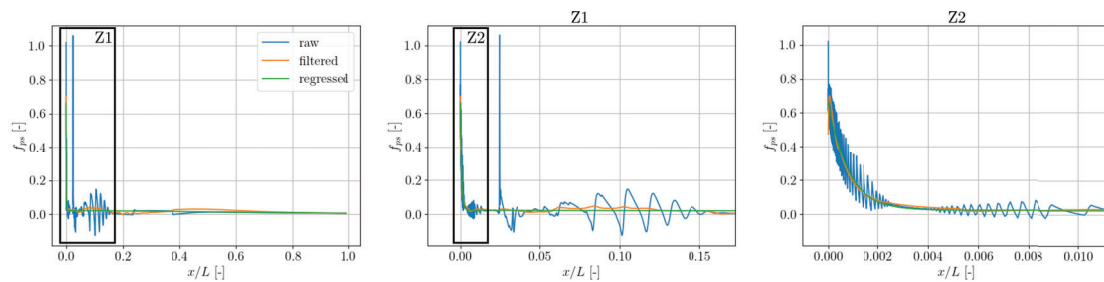


Figure 4: Shear coefficient calculated from the raw and filtered total pressure field from figure 3 with equation (13). The exponential decay at the inlet is attributed to a separation bubble at the exit of the primary nozzle. The calculation on the raw signal suffers from sharp gradients in the shock train and the Mach disk ($x/L = 0.025$). The physics-separated regression is carried out with equation (15) on the filtered shear coefficient f_{ps} .

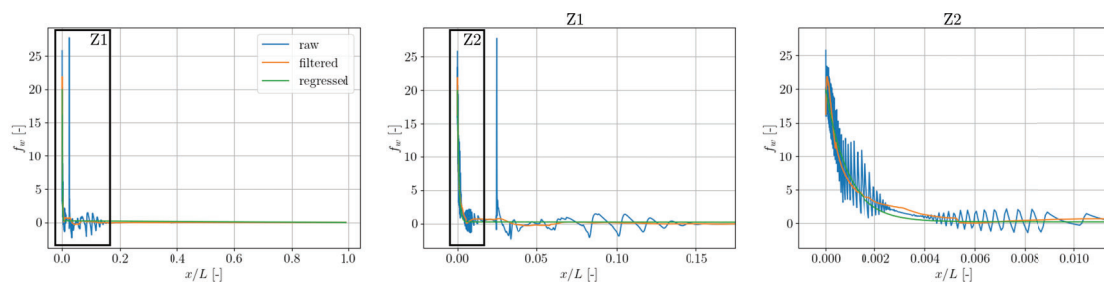


Figure 5: Wall friction coefficient calculated from the raw and filtered total pressure field from figure 3 with equation (13). The same trends are observed for the shear between the streams (cf. figure 4), so the same parametric function is used for the regression.

Next, we use the regressed closure relation to predict the flow field of the ejector with the 1D model. The resulting flow field compares well to the post-processed CFD (cf. figure 6). Upstream, the cross-section is imposed by the CFD, leading to a close match. Downstream, the unique pressure deviates from the values in the CFD due to the shock train (the primary stream is particularly affected). Nevertheless, the 1D model captures the global rising trend. This pressure increase arises from the momentum exchange between the two streams of the compound flow (cf. equation (6) with $\beta > 0$). The pressure rises more strongly in the diffuser from $x/L = 0.23$ and reaches a constant value where the streams reach the same total pressure. The constant total temperature in the 1D-2s model matches the post-processed CFD within 3 K. The deviation is attributed to the low enthalpy in the separation bubble at the exit of the primary nozzle, which influences the total temperature field downstream near the dividing streamline. The constant total temperature remains a good approximation for the bulk of the streams. Thermal mixing through different inlet temperatures is foreseen as a future extension of the 1D-2s model.

Despite the indirect penalization on the closure coefficients, an excellent match is obtained. The assumption of equal static pressure in both streams proves to be an acceptable assumption to close the system of equations (6)-(11) (at least in this off-design operating point). The match of the cross-sections between the 1D model and the CFD best validates the model. However, the 1D model shows a mismatch in back pressure (2.3 bar in the model and 2.2 bar in the CFD). The formulation with the ODEs always requires a shooting method to match a boundary condition at the exit of the domain ($x = L$), but none of the flow quantities is penalized in the physics-separated approach. Therefore, we apply the physics-integrated method in the next section to improve the prediction in the flow quantities both in the internal domain and the boundary condition for the static pressure.

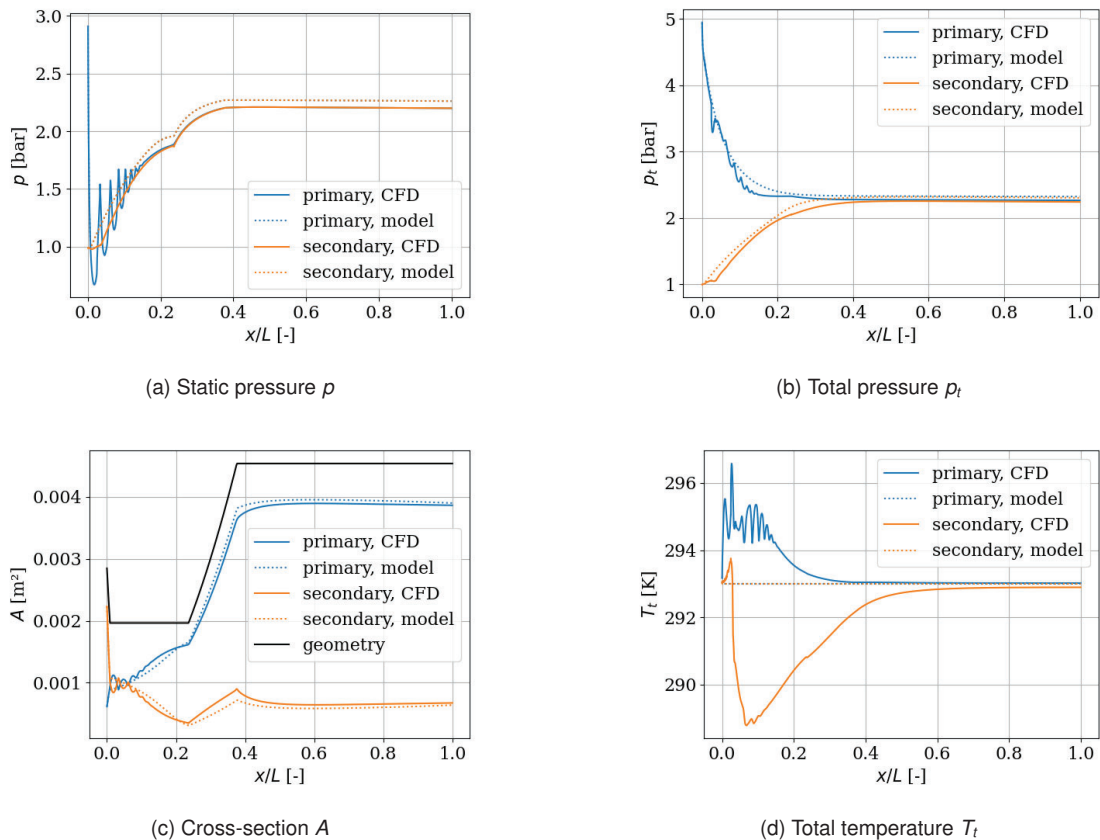


Figure 6: Model predictions with the regressed closure relation from the physics-separated approach (cf. figures 4 and 5). All variables match the post-processed 1D data quite well (the cost function (14) equals 0.0044). However, the boundary condition of the static pressure at the outlet is not met due to the indirect regression on the post-processed closure coefficients instead of on the physical quantities (cf. equations (2) and (14)).

4.2. Physics-integrated approach

The closure relation from the section above serves as an initial guess for the physics-integrated approach, where the prediction error on the physical quantities is minimized (including the back pressure as a boundary condition, cf. equation (14)). The resulting evolution of the shear and friction coefficients is shown in figure 7. The wall friction coefficient increased significantly, resulting in lower static pressure and a satisfied boundary condition (cf. figure 8a). An increased shear coefficient compensates for the corresponding loss in secondary total pressure. Finally, we note that the exponential decay between the inlet and $x/L = 0.01$ from figures 4 and 5 has sharpened, which results in a flat plateau in the coefficients in figure 7. This indicates the extreme values found with the physics-separated approach were not necessary.

The physics-integrated approach has decreased the value of the cost function (equation (14)) from 0.0044 with the initial guess from the physics-separated approach to 0.0036. This significant improvement can be appreciated visually by comparing figures 6 and 8. However, the integrated approach is less straightforward

a priori; one does not know which type of parametric function allows a close match. Additionally, initializing the weights is also non-trivial. For example, an excessive wall friction coefficient could decrease the static pressure enough to choke the flow and lead to problems in the integration of the system of ODEs (which becomes singular if $\beta = 0$). Therefore, the initialization through the physics-separated approach followed by fine-tuning with the physics-integrated proves an effective strategy for the model calibration, profiting from their complementary advantages.

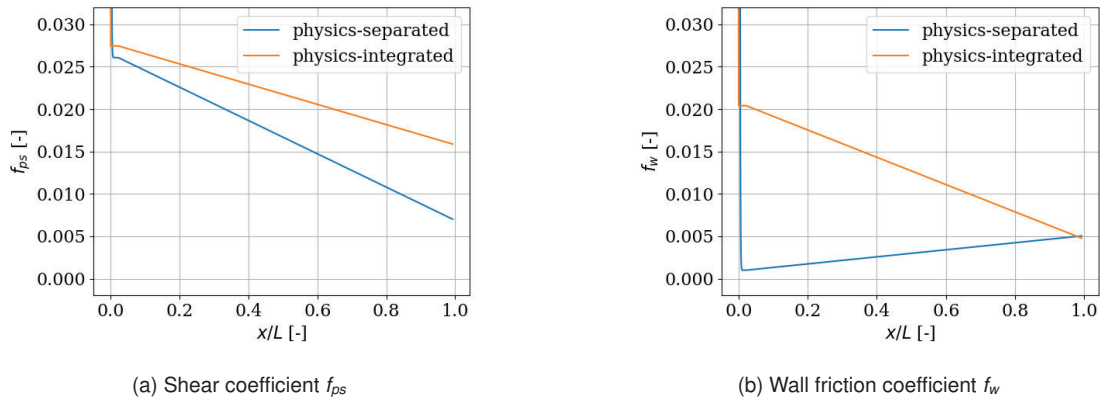


Figure 7: Comparison of the regressed closure relations of the physics-separated and the physics-integrated approach. The first serves as initial guess for the latter method and is optimized to minimize cost function (14) (final value of 0.0036). A significant increase of the wall friction coefficient has allowed to decrease the static pressure in the mixing duct, leading to a satisfied boundary condition (cf. figure 8a).

5. Conclusion

This work proposes a general machine learning framework for calibrating physical models governed by a system of ODEs. We have explored a physics-separated approach, which consists of calculating the closure coefficients from higher resolution data (CFD) and then regressing the post-processed coefficients, and a physics-integrated approach, where the model is called upon during the optimization (training) phase to minimize the prediction error on the observed physical quantities. Both approaches have been applied successfully on a 1D ejector model to find the shear and wall friction coefficients as a function of the spatial coordinate.

The results show that a successive application of both approaches proves to be a convenient and robust method to calibrate the 1D model. The physics-separated approach guides the choice of the parametric function and provides a valid initial guess for the physics-integrated approach. This then acts as a refinement tool to further minimize the prediction error by *directly* penalizing mispredictions in the state variables.

The proposed methodology is robust and flexible: it is compatible with state-of-the-art optimizers and leaves a free choice of the regressor. Any parametric tool fits the framework, ranging from linear regression to artificial neural networks. Furthermore, the method brings physical insight through closure relations for low-order but highly interpretable models. Finally, the framework can be categorized as *physics-constrained*, as opposed to *physics-informed*, machine learning since the conservation equations are always respected. From a more global perspective, splitting the problem in a set of physical equations f and closure relations g (cf. equation (1)) allows the continued use of dedicated solvers for the physical problem f , which are conservative and efficient, and simplifies the machine learning task by restricting its scope to the closure problem g . In this sense, the framework is an extension of neural ODEs, which solve the combined problem of f and g with neural networks without including prior physical knowledge. Consequently, less complex regressors may suffice for solving the problem, reducing the amount of required data or improving the performance on a fixed dataset.

Improvements are foreseen on two fronts. Firstly, the 1D ejector model is currently being extended to on-design operation with a pressure equalization mechanism to remove the requirement of imposing the cross-section from CFD at the inlet of the mixing pipe. Secondly, the adjoint method is being explored to handle closure laws requiring many weights (e.g., neural networks). Finally, the closure coefficients can be linked to the state variables rather than space coordinates to discover more universal closure relations for the 1D ejector model. This will require an extensive study on operating conditions and various geometries.

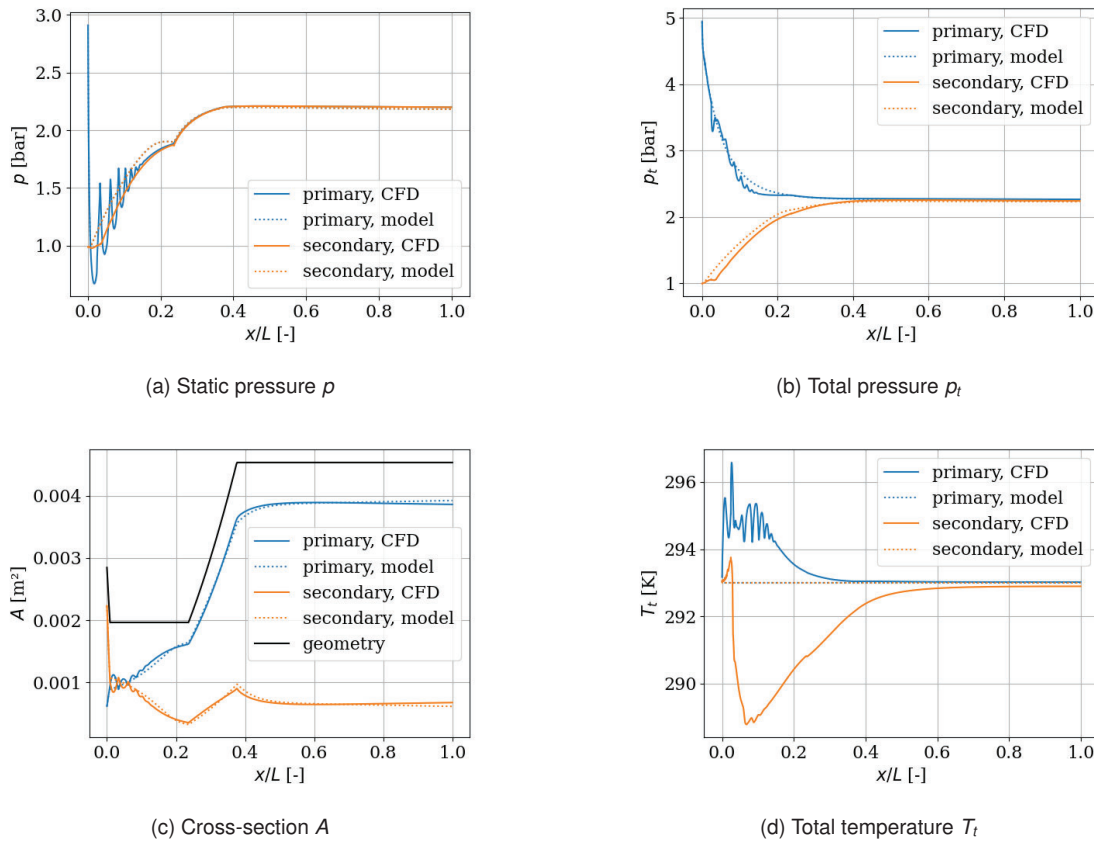


Figure 8: Model predictions with the regressed closure relation from the physics-integrated approach (cf. figure 7). The agreement improved compared to the physics-separated approach in figure 6 (the cost function (14) equals 0.0036). Moreover, the boundary condition of the static pressure at the outlet is now respected.

Acknowledgments

J. Van den Berghe is supported by a F.R.S.-FNRS FRRIA grant. This project has received funding from the Clean Sky 2 Joint Undertaking (JU) under grant agreement No 101008100. The JU receives support from the European Union's Horizon 2020 research and innovation programme and the Clean Sky 2 JU members other than the Union.

Disclaimer: The contents presented in this article reflect only the author's point of view: the authors and Clean Sky JU are not responsible for any use that may be made of the information it contains.

Appendix A Derivation of the 1D ejector model from first principles

The base equations of the 1D model are the quasi-1D Euler equations with a force term F :

$$d_x(\rho_i A_i V_i) = 0; \quad d_x(\rho_i A_i V_i^2) = -A_i d_x p_i + F_i; \quad d_x(\rho_i A_i V_i h_{ti}) = 0 \quad (16)$$

where the index i denotes either the primary (p) or the secondary stream (s). The following equivalent system can be derived from these conservation equations (cf. [26] for a detailed derivation):

$$\frac{d_x p_i}{p_i} = \left[\frac{1 + (\gamma - 1) M_i^2}{1 - M_i^2} \right] \frac{F_i}{A_i p_i} + \left[\frac{\gamma M_i^2}{1 - M_i^2} \right] \frac{d_x A_i}{A_i}, \quad \frac{d_x p_{ti}}{p_{ti}} = \frac{F_i}{A_i p_i}, \quad \frac{d_x T_{ti}}{T_{ti}} = 0 \quad (17)$$

The wall friction force acts on the secondary stream and is defined through a classic friction coefficient:

$$F_w = -\frac{1}{2} f_w \rho_s V_s^2 = -\frac{1}{2} f_w \gamma p_s M_s^2 \quad (18)$$

The shear force is defined in a similar way and depends on the difference in dynamic pressure:

$$F_{ps} = \frac{1}{2} f_{ps} (\rho_p v_p^2 - \rho_s v_s^2) = \frac{1}{2} f_{ps} \gamma \rho (M_p^2 - M_s^2) \quad (19)$$

The primary and secondary forces are given by $F_p = -F_{ps}$ and $F_s = F_{ps} + F_w$. Combining the equations above results in equations (7) and (8). The equation for the static pressure results from the assumption of equal static pressure in both streams. The first step is to inverse equation (17) in terms of the area:

$$d_x A_i = \left[A_i \frac{1 - M_i^2}{\gamma M_i^2} \right] \frac{d_x p}{\rho} - \left[\frac{1 + (\gamma - 1) M_i^2}{\gamma M_i^2} \right] \frac{F_i}{\rho} \quad (20)$$

where the static pressure p lost the index because we assume $p_p = p_s$. Equations (10) and (11) for the gradient of the cross-sections follow from the equation above after filling in the forces. We sum the equation above for both streams and obtain the gradient of the known geometry $A = A_p + A_s$:

$$d_x A = \left[A_p \frac{1 - M_p^2}{\gamma M_p^2} + A_s \frac{1 - M_s^2}{\gamma M_s^2} \right] \frac{d_x p}{\rho} - \left[\frac{1 + (\gamma - 1) M_p^2}{\gamma M_p^2} \right] \frac{F_p}{\rho} - \left[\frac{1 + (\gamma - 1) M_s^2}{\gamma M_s^2} \right] \frac{F_s}{\rho} \quad (21)$$

The first term corresponds to the compound choking indicator β from equation (12). We reverse the equation above, to obtain the following expression of the pressure gradient:

$$\frac{d_x p}{\rho} = \frac{1}{\beta} \left(d_x A + \left[\frac{1 + (\gamma - 1) M_p^2}{\gamma M_p^2} \right] \frac{F_p}{\rho} + \left[\frac{1 + (\gamma - 1) M_s^2}{\gamma M_s^2} \right] \frac{F_s}{\rho} \right) \quad (22)$$

Equation (6) follows after filling in the forces and some simplifying operations.

Nomenclature

Letter symbols

e	specific internal energy, J/(kgK)
f_{ps}	shear coefficient, –
f_w	wall friction coefficient, –
l_{ps}	perimeter of the primary cross-section, m
l_w	perimeter of the wall, m
\dot{m}	mass flow rate, kg/s
p	pressure, Pa
r	radial coordinate, m
t	time, s
u	axial velocity, m/s
x	axial coordinate, m
A	cross-section, m ²
F	force per unit length, N/m
L	length of the ejector, m
M	Mach number, –
R	wall radius, m

T	temperature, K
\mathbf{p}	vector of closure parameters, –
\mathbf{u}	state vector, –
\mathbf{w}	weight vector, –

Greek symbols

β	compound choking indicator, m ²
γ	ratio of specific heat capacities (air: 1.4), –
ρ	density, kg/m ³

Subscripts and superscripts

$\hat{\cdot}$	cross-sectional average of a variable
$\bar{\cdot}$	observation of a variable
b	back, outlet of the ejector
p	primary stream
s	secondary stream
t	total quantity (pressure, temperature, internal energy)

References

- [1] Aidoun Z., Ameer K., Falsafioon M., Badache M., *Current advances in ejector modeling, experimentation and applications for refrigeration and heat pumps. Part 1: Single-phase ejectors*. *Inventions* 2019;4(1):15.
- [2] Keenan J. H., Neumann E. P., *A Simple Air Ejector*. *Journal of Applied Mechanics* 1942;9(2):A75-A81.
- [3] Munday J. T., Bagster D. F., *A New Ejector Theory Applied to Steam Jet Refrigeration*. *Industrial & Engineering Chemistry Process Design and Development* 1977;16(4):442-449.
- [4] Eames I. W., Aphornratana S., Haider H., *A theoretical and experimental study of a small-scale steam jet refrigerator*. *International journal of refrigeration* 1995;18(6):378-386.

- [5] Chen W., Liu M., Chong D., Yan J., Little A. B., Bartosiewicz Y., *A 1D model to predict ejector performance at critical and sub-critical operational regimes*. International Journal of Refrigeration 2013;36(6):1750-1761.
- [6] Metsue A., Debroyer R., Poncet S., Bartosiewicz Y., *An Improved Thermodynamic Model for Supersonic Real-Gas Ejectors using the Compound-Choking Theory*. Energy 2021;238:121856.
- [7] Bartosiewicz Y., Aidoun Z., Desevaux P., Mercadier Y., *Numerical and experimental investigations on supersonic ejectors*. International Journal of Heat and Fluid Flow 2005;26(1):56-70.
- [8] Hemidi A., Henry F., Leclaire S., Seynhaeve J., Bartosiewicz Y., *CFD analysis of a supersonic air ejector. Part I: Experimental validation of single-phase and two-phase operation*. Applied Thermal Engineering 2009;29(8):1523-1531.
- [9] Van den Berghe J., Dias B. R. B., Bartosiewicz Y., Mendez M. A., *A 1D model for the unsteady gas dynamics of ejectors*. Energy 2023;267:126551.
- [10] Clark L., *Application of compound flow analysis to supersonic ejector-mixer performance prediction*. In: 33rd Aerospace Sciences Meeting and Exhibit; 1995; 645.
- [11] Banasiak K., Hafner A., *1D Computational model of a two-phase R744 ejector for expansion work recovery*. International Journal of Thermal Sciences 2011;50(11):2235-2247.
- [12] del Valle J. G., Jabardo J. M. S., Ruiz F. C., Alonso J. S. J., *A one dimensional model for the determination of an ejector entrainment ratio*. International Journal of Refrigeration 2012;35(4):772-784.
- [13] Berg J., Nyström K., *Neural network augmented inverse problems for PDEs*. arXiv preprint arXiv:1712.09685 2017.
- [14] Parish E. J., Duraisamy K., *A paradigm for data-driven predictive modeling using field inversion and machine learning*. Journal of computational physics 2016;305:758-774.
- [15] Holland J. R., Baeder J. D., Duraisamy K., *Field inversion and machine learning with embedded neural networks: Physics-consistent neural network training*. In: AIAA Aviation 2019 Forum; 2019.
- [16] Sirignano J., MacArt J. F., Freund J. B., *DPM: A deep learning PDE augmentation method with application to large-eddy simulation*. Journal of Computational Physics 2020;423:109811.
- [17] MacArt J. F., Sirignano J., Freund J. B., *Embedded training of neural-network subgrid-scale turbulence models*. Physical Review Fluids 2021;6(5):050502.
- [18] Sirignano J., MacArt J., Spiliopoulos K., *PDE-constrained models with neural network terms: optimization and global convergence*. arXiv preprint arXiv:2105.08633 2021.
- [19] Chang C., Dinh N. T., *Classification of machine learning frameworks for data-driven thermal fluid models*. International Journal of Thermal Sciences 2019;135:559-579.
- [20] `scipy.optimize.minimize` Available at: <https://docs.scipy.org/doc/scipy/reference/generated/scipy.optimize.minimize.html> [accessed 7 March 2023].
- [21] Mendez M. A., Dominique J., Fiore M., Pino F., Sperotto P., Van den Berghe J., *Challenges and Opportunities for Machine Learning in Fluid Mechanics*. In: Proceedings of the 19th International Topical Meeting on Nuclear Reactor Thermal Hydraulics (NURETH); 2022. Preprint at arXiv 2202.12577.
- [22] Schillaci E., Olié Casasayas C., Vemula J. B., Duponcheel M., Bartosiewicz Y., Planquart P., *Air Ejector Analysis in Normal and Abnormal Modes, Oriented to Control Purposes in Aircraft Systems*. In: 9th European Conference for Aeronautics and Space Sciences (EUCASS); 2022; European Conference for AeroSpace Sciences (EUCASS); 2022; 1-12.
- [23] Lamberts O., Chatelain P., Bourgeois N., Bartosiewicz Y., *The compound-choking theory as an explanation of the entrainment limitation in supersonic ejectors*. Energy 2018;158:524-536.
- [24] Bernstein A., Heiser W. H., Hevenor C., *Compound-compressible nozzle flow*. 1967.
- [25] Croquer S., Fang Y., Metsue A., Bartosiewicz Y., Poncet S., *Compound-choking theory for supersonic ejectors working with real gas*. Energy 2021;227:120396.
- [26] Shapiro, A. H., *Generalized one-dimensional continuous flow*. In: The dynamics and thermodynamics of compressible fluid flow. New York: Ronald Press. 1953. p. 219-262.